SHORT REPORT
doi: 10.2306/scienceasia1513-1874.2023.086

ScienceAsia 49 (2023): **859–863**

The role of carbon electrode parameters on capacitive deionization efficiency

Kunchaya Thungsuai, Nuttaporn Pimpha, Saowaluk Chaleawlert-umpon*

National Nanotechnology Center, National Science and Technology Development Agency, Thailand Science Park, Pathum Thani 12120 Thailand

*Corresponding author, e-mail: saowaluk@nanotec.or.th

Received 24 Feb 2023, Accepted 27 Aug 2023
Available online 22 Nov 2023

ABSTRACT: Capacitive deionization (CDI) is an alternative promising desalination technology due to its environmentally friendly and cost-effective process. In this study, the effects of carbon electrode parameters, such as porous carbon layer thickness and water channel gap distance on CDI efficiency, were systematically evaluated in terms of salt adsorption capacity (SAC). In addition, kinetic salt adsorption rate was discussed. The study demonstrated that appropriate carbon layer thickness of electrode and gap distance between electrodes were crucial parameters for CDI cell fabrication to optimize the desalination performance.

KEYWORDS: capacitive deionization, desalination, porous carbon electrode

INTRODUCTION

Capacitive deionization (CDI) is a promising alternative technology for water desalination. With respect to cost-effective and environmentally friendly process, CDI is claimed to be more effective approach for desalination of water with low and moderate salt content than traditional technologies such as ion exchange, electrodialysis, and reverse osmosis [1, 2]. The CDI technology is based on an electrochemically controlled process via an electrical double layer (EDL) mechanism. It is operated at a relatively low electrical voltage (typically 0.8–1.6 V) to safely and easily drive the adsorption of charge ions by electrostatic force attraction, resulting in the removal of ions from the feed water.

In general, the adsorption performances of CDI mainly depend on the nature of electrode materials such as surface area, pore size, and electrical conductivity. The most preferred electrode material would have high surface area of porous carbon groups contributing to good electrical conductivity and low cost. Most studies focused on novel activated carbon materials to improve an electrosorption capacity as much as possible [3–5]. However, the carbon electrode property may differ from pristine carbon due to electrode fabrication parameters. In the literature, there have been few relevant studies focusing on the carbon electrode property. In this short report, we explored how the porous carbon layer thickness on the electrode and gap distance for water flow channel between a pair of electrodes affected the electrosorption performance, such as adsorption capacity and adsorption rate, in the CDI process. We believed that the study could provide invaluable findings concerning the impact of electrode fabrication parameters for further optimizing the CDI process.

MATERIALS AND METHODS

Materials

Power activated carbon (PC) was received from Right Solution Co., Ltd., Bangkok, Thailand. Conductive graphite powder was purchased from MTI Corporation, CA, USA. Polytetrafluoroethylene (60 wt% H_2O) (PTFE) and ethanol (EtOH) were received from Aldrich, MA, USA.

Methods

Electrode preparation

A typical procedure available in the literature was used for the preparation of carbon-based electrode [6–8]. Briefly, PC, conducting graphite, and PTFE in a mass ratio of 80:5:15, respectively, were mixed together and formed a dough-like mixture with EtOH. The mixture was, then, spreaded evenly onto a graphite sheet with a geometric surface area of 1×1 cm^2 (for electrochemical tests) and 8×8 cm^2 (for CDI measurements). The porous carbon layer thickness was controlled by a plastic frame during the kneading and rolling of the mixture onto the graphite sheet. The electrodes were dried in an oven at 120 °C for 24 h.

Material characterization

The surface morphology and thickness of the porous carbon electrodes were determined by scanning electron microscopy and energy dispersive X-ray spectrometer (SEM-EDX, Hitachi SU8030). Nitrogen adsorption measurements were performed using Micromeritics 3Flex 3500 with N_2 at 77 K. Prior to the analyses, the porous carbon electrodes (1×1 cm^2) were degassed under vacuum at 180 °C for 3 h. The specific surface area was calculated by applying the Brunauer-Emmett-

Teller (BET) model. Electrochemical behavior was determined by electrochemical impedance spectroscopy (EIS) and cyclic voltammetry (CV) using a potentiostat (Palmsens, Palmsens4). All measurements were performed in a conventional three-electrode system. The sample was used as a working electrode, Ag/AgCl (saturated KCl) as a reference electrode, and Pt wire as a counter electrode. EIS was conducted in 0.5 M NaCl solution with the frequency range of 0.01–100 kHz with 10 mV sinusoidal voltage. The areal capacitance (C, F/cm^2) of the electrodes was obtained by Eq. (1):

$$C = \frac{\int_{E_1}^{E_2} I \, dE}{2a\,\nu(E_2 - E_1)} \tag{1}$$

where E_1 and E_2 are the lower and upper of working potential window (V), I is the current (A), a is the active area of electrode (cm^2), and ν is the scan rate (V/s).

CDI experiments

The porous carbon electrodes were assembled into a self-made CDI apparatus with batch mode operating. All experiments were operated with a flow rate of 30 ml/min in a 500 mg/l NaCl solution with a volume of 140 ml. A direct voltage was applied on the opposite electrodes. The NaCl concentration was calculated by a standard calibration curve between the conductivity and the concentration of NaCl solutions. Removal efficiency and salt adsorption capacity (SAC, mg/g) were defined by Eqs. (2) and (3), respectively:

$$\text{Removal efficiency (\%)} = \frac{C_0 - C_e}{C_0} \times 100 \tag{2}$$

$$\text{SAC} = \frac{(C_0 - C_e)V}{m} \tag{3}$$

where C_0 and C_e are the initial and final NaCl concentrations (mg/l), V is the volume of the NaCl solution (l), and m is the total mass of the electrodes (g). The charge efficiency was calculated according to Eq. (4):

$$\text{Charge efficiency} = \frac{\text{SAC} \times F}{\Sigma} \tag{4}$$

where F is the Faraday constant (96,485 C/mol), SAC is the electrosorption capacity (mol/g) and Σ is the charge (C/g) obtained by integrating the corresponding current. The kinetic rate constant was calculated from the pseudo-first-order equation (5):

$$\log(q_e - q_t) = \log q_e - \frac{kt}{2.303} \tag{5}$$

where q_e is the saturated SAC (mg/g), q_t is the SAC at different times (mg/g), k is the rate constant (min^{-1}), and t is the adsorption time (min).

RESULTS AND DISCUSSION

A diagram showing the system setup in batch mode (cycling) was depicted in Fig. 1a. The assembled CDI unit cell was composed of two porous carbon electrodes separated by a silicone sheet acting as a channel for water flow. The current collectors were used as a supporter for the porous carbon-based electrode. Fig. 1b shows the electrode parameters: porous carbon layer thickness and water channel gap distance that were studied in this report.

Surface morphology was analyzed using SEM. The top view image (Fig. 2a) exhibits the irregular shape of PC, and the corresponding EDX image (Fig. 2b) shows the detected elements of C and F. It was confirmed that the PTFE binder was randomly distributed on the PC particles. The cross-sectional images in Fig. 2c-e present the thickness of porous carbon layer on the graphite sheet in approximate thicknesses of 300, 600, and 800 µm. Therefore, the tested porous carbon electrodes were labeled E-thin, E-mid, and E-thick, respectively. The specific surface area of the porous carbon electrodes had a significant difference from pristine PC. They were 380, 480, and 574 m^2/g for E-thin, E-mid, and E-thick, respectively; which were reduced approximately 50–67% as compared with pristine PC (1,155 m^2/g). Reducing the surface area of the porous carbon electrodes was mainly because of PTFE binder covering for holding all PC particles together on the film structure, resulting in the pore blocking.

To probe the internal resistance of the porous carbon electrodes, EIS spectroscopy was conducted in 0.5 M NaCl for clear observation. Nyquist plots of the electrodes were presented in Fig. 2a. The Nyquist plot of the EDL electrode materials generally consists of a vertical line in a low-frequency region, corresponding to capacitive behavior and a semicircle in a high-frequency region, indicating electrolyte resistance. Additionally, an x-intercept value refers to the total internal resistance implying an electrode material resistance when all experiments were performed under identical environments. The vertical line of all electrodes exhibited almost the same steep slope indicating EDL formation control; whereas, the E-thin had a lower x-intercept value and a smaller diameter of semicircle than those of the thicker electrodes. This suggested that the internal resistance decreased with a decrease of porous carbon layer thickness on the electrode. The result indicated that the mobility of electrolytes in the textural pores was facilitated by the short diffusion path [9, 10] and a small contact resistance between the current collector and the active material interface [11].

The electrochemical property of the porous carbon electrodes was studied by cyclic voltammetry (CV) in a low concentrat ion of electrolyte (10 mM NaCl solution was used for relative electrolyte with CDI experiment). The voltammograms (Fig. 3b) shows an oval shape without a redox peak indicating their charge storage

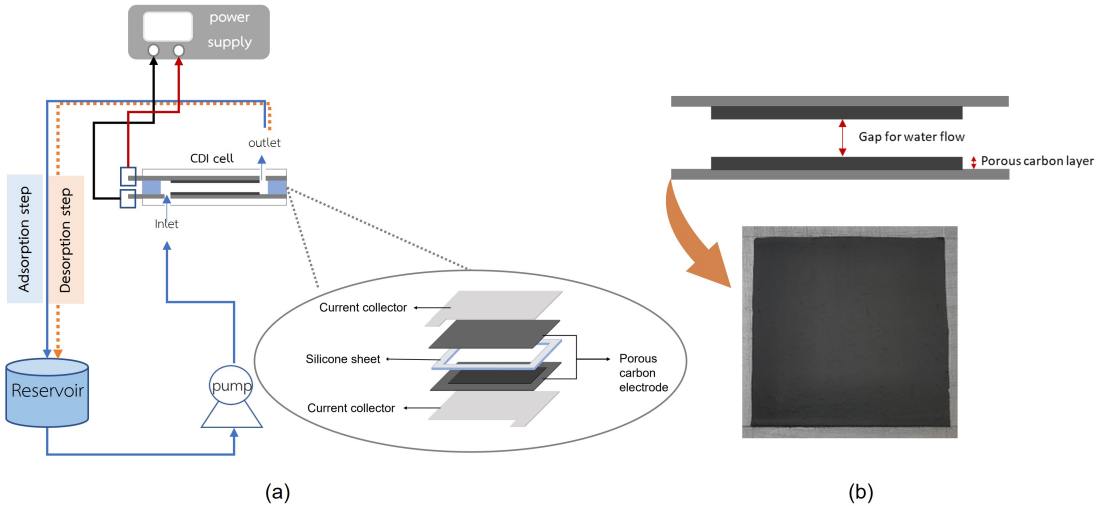

Fig. 1 (a) Diagram for CDI setup system and CDI unit cell configuration; and (b) gap for water flow between a pair of electrodes (an image of porous carbon electrode).

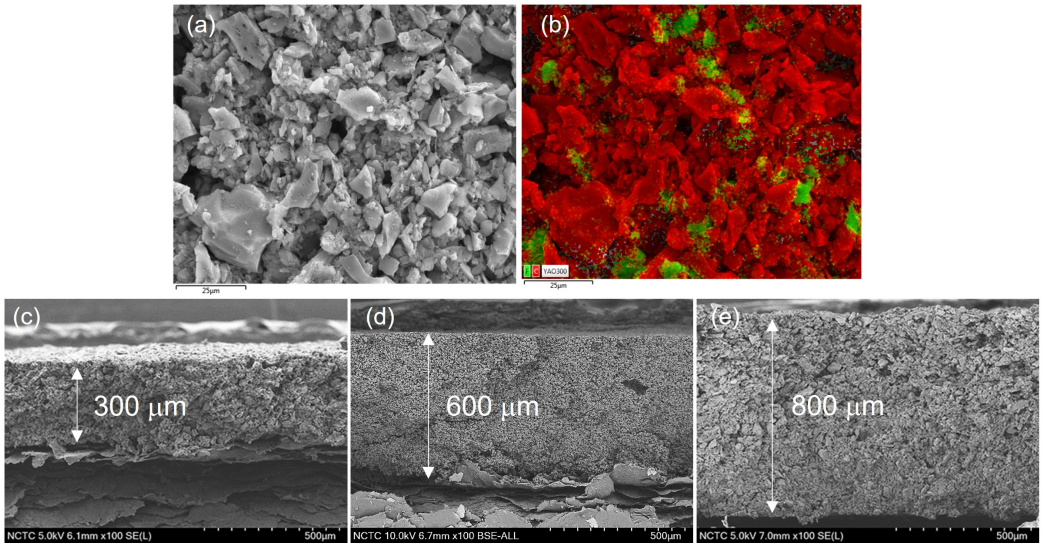

Fig. 2 SEM images: (a) top view of the porous carbon electrode; (b) the corresponding EDX mapping with C (red) and F (Green) elements; and (c-e) cross-section views indicating the thickness of various porous carbon layer.

ability through EDL process [3]. The corresponding areal capacitances were 81, 72, and 50 mF/cm^2 for E-thin, E-mid, and E-thick, respectively. As a result, the increase of porous carbon layer thickness on the electrode led to the decrease of areal capacitance owing to increasing internal resistance.

To study salt adsorption efficiency, CDI experiments were performed at a constant voltage and batch mode experiment. We first investigated the effect of operating voltage on the electrosorption performances of E-thin in a 500 mg/l NaCl solution. Fig. 3c shows the conductivity change during the adsorption process of different voltages: the solution conductivity decreased sharply and then reached an equilibrium state. With increasing operating voltage, the removal efficiency increased from 10% to 30% owing to high voltages inducing high electrostatic forces between the electrode surface and ions [3, 12, 13]. However, salt adsorption capacity reached the highest value at 4.1 mg/g when the applied voltage was at 1.2 V. A higher applied voltage over 1.2 V did not yield a greater salt adsorption capacity possibly due to the side reactions occurring at the high voltages [12, 14, 15]. So, the applied voltage of 1.2 V would be used as adsorption operating voltage in the other CDI experiments. Fig. 3d exhibits the conductivity profile in a single CDI cycle with

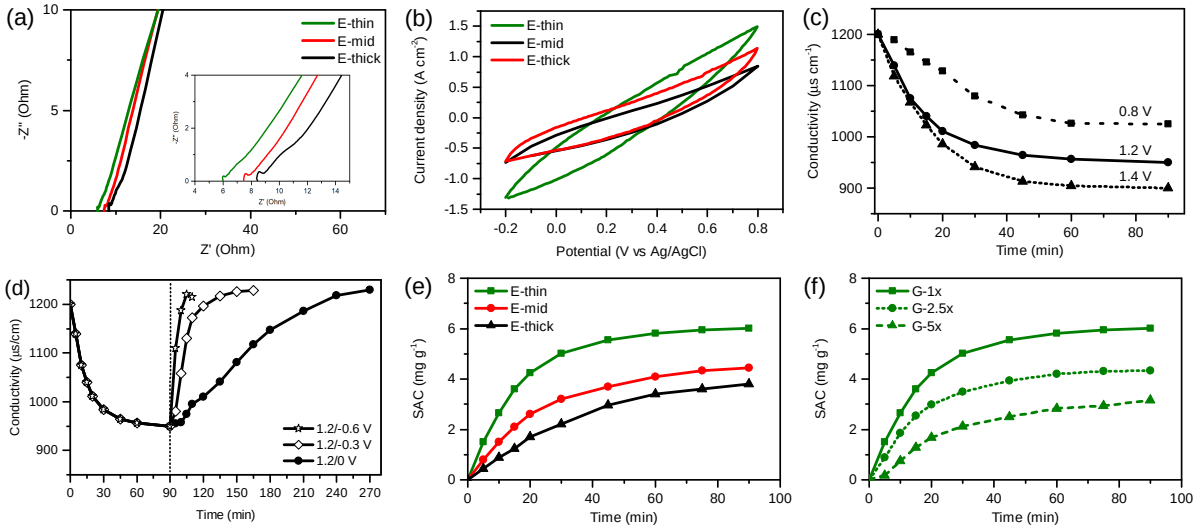

Fig. 3 Electrochemical tests: (a) Nyquist plots analyzed in a 0.5 M NaCl solution; and (b) CV curves performed at a scan rate of 10 mV/s in a 10 mM NaCl solution. Conductivity profiles: (c) different applied voltages for adsorption and (d) different applied voltages for desorption with using 1.2 V operating voltage for adsorption. Salt adsorption capacity as a function of time: (e) the different porous carbon layer thicknesses; and (f) the variation of gap distance between a pair of E-thin electrodes. All electrosorption performances were analyzed in a 500 mg/l NaCl solution.

Table 1 CDI performances with variation of porous carbon layer thicknesses and gap distances of the CDI electrodes.

Sample	SAC(mg/g)	Charge efficiency	Pseudo-first-order model		
			k(min^{-1})	q_e(mg/g)	r^2
E-thin	5.61 ± 0.43	0.51 ± 0.03	0.058	5.92	0.9982
E-mid	3.93 ± 0.10	0.25 ± 0.01	0.042	4.44	0.9972
E-thick	3.77 ± 0.55	0.22 ± 0.03	0.040	4.38	0.9896
G-1x	5.61 ± 0.43	0.51 ± 0.06	0.058	5.92	0.9982
G-2.5x	4.34 ± 0.74	0.18 ± 0.03	0.052	4.24	0.9957
G-5x	2.73 ± 1.15	0.06 ± 0.05	0.037	3.32	0.9953

an operating voltage of 1.2 V during the adsorption step and a variation of desorption voltages (0, −0.3, −0.6 V). After the conductivity reached a plateau at adsorption equilibrium, the conductivity increased again until reaching approximately initial conductivity. All desorption voltages presented a desorption time difference, but they were not significantly different in electrosorption capacity. Due to an appropriate desorption time, the desorption operating voltage at −0.3 V was selected.

Subsequently, the CDI performances over the different porous carbon layer thicknesses of the electrodes were evaluated. Fig. 3e presents a variation of the salt adsorption capacity with the operating time of all electrodes. It was found that the salt adsorption capacity increased steeply at the initial time and then reached an adsorption equilibrium after 60 min for E-thin. Besides, the salt adsorption profile of the thicker electrodes (E-mid and E-thick) illustrated a similar pattern with a slow adsorption rate and gradually almost constant around 90 min. The corresponding salt adsorption capacity values were summarized in Table 1, in accordance with the results analyzed using the pseudo-first-order adsorption kinetic model. All samples had a regression that fitted well with the pseudo-first-order model and verification r^2 values above 0.98. E-thin had the highest salt adsorption capacity value (5.61 mg/g) and a faster adsorption rate constant (0.058 min^{-1}) compared with the other electrodes. E-mid and E-thick had almost similar salt adsorption capacity values of 3.93 mg/g and 3.77 mg/g, respectively. It was suggested that a saturation of salt adsorption capacity occurred due to a limitation of long ion pathways into the porous carbon structure layer of the thicker electrodes. Therefore, it confirmed that E-thin had a better electrosorption performance in terms of salt adsorption capacity and salt adsorption rate than the thicker electrodes.

To further study another parameter, the effect of gap distance for water flow channel on electrosorption performances was tested. The gap between a pair of electrodes was varied: 1 (G-1x), 2.5 (G-2.5x), and 5 (G-5x) times thickness of E-thin (300 µm). The results of the salt adsorption capacity as an influence of gap channel distancing were presented in Fig. 3f and Table 1. It was found from the electrosorption performances of E-thin with different gap distances that the increase of gap distance reduced the salt adsorption efficiency. Moreover, the adsorption rate constant of G-1x showed the highest value, indicating the fastest adsorption process among the different tested gap distances. The wider channel created a

longer ion diffusion distance from water stream to the electrodes and a weaker electric field strength [16, 17]. So, it was confirmed that a narrow gap distance for water flow channel contributed to the highly efficient electrosorption performance.

Furthermore, charge efficiency with respect to energy consumption efficiency was shown in Table 1. We observed a relatively higher charge efficiency of the thinner electrode than those of the thick electrodes; while the narrower gap distance revealed a significantly higher charge efficiency compared with the wider distances. Therefore, it suggested that the high charge efficiency was associated with the electrode parameters: the thin porous carbon layer on the electrode and the narrow gap between a pair of electrodes.

CONCLUSION

The present study investigated the effect of two carbon electrode parameters: porous carbon layer thickness and the gap distance between a pair of electrodes on salt adsorption efficiency. CDI performances revealed that the increase in porous carbon layer thickness of the electrode reduced the capacity and the rate of salt adsorption. It originated from the limitation of the long ion pathways into the porous structure of the thick carbon layer electrode. For gap distance, the narrow distance between a pair of electrodes facilitated the high electrosorption performance, a result of the strong electrical field. Therefore, the appropriate thickness of the electrode and gap distance for CDI unit cell assembly would optimize capacitive deionization efficiency for further practical application.

Acknowledgements: This work was financially supported by National Research Council of Thailand (NRCT) (Grant number 2558864, 2021).

REFERENCES

1. Anderson MA, Cudero AL, Palma J (2010) Capacitive deionization as an electrochemical means of saving energy and delivering clean water. Comparison to present desalination practices: Will it compete? *Electrochim Acta* **55**, 3845–3856.
2. Porada S, Zhao R, van der Wal A, Presser V, Biesheuvel PM (2013) Review on the science and technology of water desalination by capacitive deionization. *Prog Mater Sci* **58**, 1388–1442.
3. Chaleawlert-umpon S, Phiromrak S, Pimpha N (2021) Sustainable *N*-doped lignin-derived porous carbon showing ion selectivity in capacitive deionization applications. *Environ Sci Water Res Technol* **7**, 1828–1839.
4. Chen Z, Ding Z, Chen Y, Xu X, Liu Y, Lu T, Pan L (2023) Three-dimensional charge transfer pathway in close-packed nickel hexacyanoferrate-on-MXene nanostacking for high-performance capacitive deionization. *Chem Eng J* **452**, 139451.
5. Wang K, Liu Y, Xu X, Jiao Y, Pan L (2023) *In situ* synthesis of ultrasmall $NaTi_2(PO_4)_3$ nanocube decorated carbon nanofiber network enables ultrafast and superstable rocking-chair capacitive deionization. *Chem Eng J* **463**, 142394.
6. Shulga YM, Baskakov SA, Kabachkov EN, Baskakova YV, Dremova NN, Koplak OV, Lobach AS, et al (2020) Preparation and characterization of a flexible rGO-PTFE film for a supercapacitor current collector. *Langmuir* **36**, 8680–8686.
7. Ozpinar P, Dogan C, Demiral H, Morali U, Erol S, Yildiz D, Samdan C, et al (2023) Effect of binder on the electrochemical performance of activated carbon electrodes obtained from waste hazelnut shells: Comparison of PTFE and PVDF. *Diamond Relat Mater* **137**, 110092.
8. Chiochan P, Suktha P, Phattharasupakun N, Duangdangchote S, Suksomboon M, Tejangkura W, Sawangphruk M (2022) Li-ion batteries of Ni-rich lithium nickel cobalt aluminium oxide coupled with high-energy lithiophilic anode. *ScienceAsia* **48**, 577–587.
9. Ke L, Lv W, Su F-Y, He Y-B, You C-H, Li B, Li Z, et al (2015) Electrode thickness control: Precondition for quite different functions of graphene conductive additives in $LiFePO_4$ electrode. *Carbon* **92**, 311–317.
10. Ogihara N, Itou Y, Sasaki T, Takeuchi Y (2015) Impedance spectroscopy characterization of porous electrodes under different electrode thickness using a symmetric cell for high-performance lithium-ion batteries. *J Phys Chem C* **119**, 4612–4619.
11. Santos C, Lado JJ, García-Quismondo E, Soria J, Palma J, Anderson MA (2018) Maximizing volumetric removal capacity in capacitive deionization by adjusting electrode thickness and charging mode. *J Electrochem Soc* **165**, E294–E302.
12. Hou C-H, Huang C-Y (2013) A comparative study of electrosorption selectivity of ions by activated carbon electrodes in capacitive deionization. *Desalination* **314**, 124–129.
13. Xu X, Tan H, Wang Z, Wang C, Pan L, Kaneti YV, Yang T, et al (2019) Extraordinary capacitive deionization performance of highly-ordered mesoporous carbon nanopolyhedra for brackish water desalination. *Environ Sci Nano* **6**, 981–989.
14. Shapira B, Avraham E, Aurbach D (2016) Side reactions in Ccapacitive deionization (CDI) processes: The role of oxygen reduction. *Electrochim Acta* **220**, 285–295.
15. Zhang C, He D, Ma J, Tang W, Waite TD (2018) Faradaic reactions in capacitive deionization (CDI)-problems and possibilities: A review. *Water Res* **128**, 314–330.
16. Liu M, Xue Z, Zhang H, Li Y (2021) Dual-channel membrane capacitive deionization based on asymmetric ion adsorption for continuous water desalination. *Electrochem Commun* **125**, 106974.
17. Zhao R, Satpradit O, Rijnaarts HHM, Biesheuvel PM, van der Wal A (2013) Optimization of salt adsorption rate in membrane capacitive deionization. *Water Res* **47**, 1941–1952.